

The Simulation–Tabulation Method for Classical Diffusion Monte Carlo

Chi-Ok Hwang,* James A. Given,† and Michael Mascagni*

**Department of Computer Science, Florida State University, 203 Love Building, Tallahassee, Florida 32306-4530; and †Angle Inc., 7406 Alban Station Court, Suite A112, Springfield, Virginia 22150*

E-mail: mascagni@cs.fsu.edu

Received November 13, 2000; revised September 14, 2001

Many important classes of problems in materials science and biotechnology require the solution of the Laplace or Poisson equation in disordered two-phase domains in which the phase interface is extensive and convoluted. Green's function first-passage (GFFP) methods solve such problems efficiently by generalizing the "walk on spheres" (WOS) method to allow first-passage (FP) domains to be not just spheres but a wide variety of geometrical shapes. (In particular, this solves the difficulty of slow convergence with WOS by allowing FP domains that contain patches of the phase interface.) Previous studies accomplished this by using geometries for which the Green's function was available in quasi-analytic form. Here, we extend these studies by using the simulation–tabulation (ST) method. We simulate and then tabulate surface Green's functions that cannot be obtained analytically. The ST method is applied to the Solc–Stockmayer model with zero potential, to the mean trapping rate of a diffusing particle in a domain of nonoverlapping spherical traps, and to the effective conductivity for perfectly insulating, nonoverlapping spherical inclusions in a matrix of finite conductivity. In all cases, this class of algorithms provides the most efficient methods known to solve these problems to high accuracy. © 2001 Elsevier Science

Key Words: simulation–tabulation; diffusion Monte Carlo; Green's function; first passage.

1. INTRODUCTION

Despite a vast amount of work on classical diffusion Monte Carlo methods [1–3] during the past 50 years, many problems of practical importance still have no rapid solution method. Examples include the solvation free energy of a molecule [4], the diffusion-limited reaction rate of a small ligand to a binding site on a macromolecule [5–8], and the fluid permeability of industrially important resins and cements [9–10].

In a mathematical context, these examples all require solution of the Laplace equation, the Smoluchowski equation, or other elliptic partial differential equations in a two-phase environment involving a highly distributed, convoluted, multiscale boundary, which, nonetheless, is locally smooth over most of its area.

Many such problems can be solved efficiently by Green's function first-passage (GFFP) algorithms [11]. These algorithms generalize "walk on spheres" (WOS) algorithms to allow first-passage (FP) domains to be not just spheres but a wide variety of geometrical shapes.

The research described here adds to a long history of applications of probabilistic potential theory to solve boundary value problems. The WOS method is often used to solve Laplace boundary value problems [12–14]. (The "walk on rectangles" [13, 15] and "walk on balls" [16] methods have also been used.) The WOS method uses only spherical FP domains. Thus, the distribution of FP position on its surface is trivial, i.e., uniform. The WOS method has been extended to obtain the conductivity of two-phase media by Kim and Torquato [17]. They obtain overall transition probabilities that obey simple Laplace equations. But they do not obtain the Green's functions needed to correctly sample the FP position; thus, these are not true GFFP methods. Early work within the GFFP paradigm sampled the FP position by combining the Metropolis method with explicit evaluation of the appropriate Green's function by performing numerical integration [11]. This procedure can be made arbitrarily accurate. However, it is computationally very expensive. Later applications used the analytic Green's function to tabulate the corresponding distribution function; this tabulation was then used in diffusion simulations to sample the first-passage point via interpolation [18, 19]. The initial tabulation takes substantial time, but need be performed only once for each geometry of interest. This tabulation method is efficient, but has heretofore been applied only to first-passage domains for which the Green's function is available in analytic form or can be reduced to quadratures.

GFFP methods simulate diffusion paths as follows: a FP sphere is drawn around the initial location of the Brownian particle. It is allowed to intersect the closest smooth regular patch of absorbing surface. This may be a patch that the Brownian particle has landed on. The resulting FP surface consists of the portion of absorbing surface inside the FP sphere, together with the portion of FP sphere outside the absorbing surface. The Brownian particle jumps to ("makes FP on") a point on the FP surface, which is determined by sampling the appropriate Laplacian Green's function. If that point lies on a surface with Dirichlet conditions, i.e., absorbing boundary conditions, the diffusion path terminates. Otherwise, it becomes the starting position of a new FP surface. The particle continues making FP jumps in this manner. In order to use the GFFP method in a particular application of the type described here, the interfacial surface must be locally simple in the sense that the Green's function be calculable fast enough that the computational price of sampling is less than that of using lower-order methods, i.e., discrete random walks.

In this paper, we develop a method, the simulation–tabulation (ST) method, that greatly extends the range of problems one can address by the GFFP method. The ST method does not require an analytic Green's function as a starting point. It uses simulation results directly to tabulate, or bin, contributions to the Green's function. It then follows the standard procedure (summarized in Section 2) for creating a distribution function tabulation from a Green's function tabulation. The ST method extends the range of diffusion problems that can be treated by GFFP in two ways. First, it allows a standard, i.e., absorbing, FP domain for which the Laplacian Green's function is not available in analytic form. Second, it allows mixed boundary conditions on the surfaces constituting the boundary of the FP domain.

Each FP jump requires the Brownian particle to make a transition either from a point in a single-phase domain to a point on the interface of that domain or from a point on that interface to a point in a single-phase domain. These FP jumps require sampling from two classes of Laplacian Green's functions corresponding to the two types of jump. Here, we apply the ST method to one Green's function of each type (see, respectively, Figs. 2 and 5). Once the surface Green's function for a local geometry has been tabulated, jumps that involve it can be treated as elementary in the quest to tame still larger classes of local surface geometries. This is the bootstrap aspect of the ST method.

This paper is organized as follows: In Section 2, we explain the use of the ST method to obtain a pair of basic Laplacian Green's functions. In Section 3, we evaluate the performance of ST methods on three paradigmatic diffusion problems: the Solc-Stockmayer problem, a simple model of diffusion-limited protein-ligand binding; the trapping rate of particles diffusing in a domain of spherical, nonoverlapping traps (this is a standard model of an extinction process in a random two-phase medium); and the effective conductivity of a two-phase medium, consisting of an ensemble of nonoverlapping, insulating spherical inclusions dispersed randomly in a matrix phase of finite conductivity σ_1 . In Section 4 we discuss the computational efficiency of the ST method, and in Section 5 we present our conclusions and recommendations for further research.

2. CONSTRUCTION BY THE SIMULATION-TABULATION METHOD OF TWO BASIC LAPLACIAN GREEN'S FUNCTIONS

In this section, at first we show the equivalence between the surface Green's function for a Laplacian in a bounded region and the FP probability distribution in an identical region for the theoretical basis of ST method and explain how the ST method obtains two Laplacian Green's functions required for the applications we study.

A branch of applied mathematics, probabilistic potential theory [20, 21], provides a detailed equivalence between an electrostatic problem and the equivalent diffusion problem. In particular, the surface Green's function for the Laplacian in a bounded region, i.e., the charge distribution on the interface, is equivalent to the FP probability distribution in an identical region.

It is useful to show this equivalence in detail in a specific set of examples. Consider the Dirichlet problem for the Laplace equation (see Fig. 1),

$$\begin{aligned}\Delta u(\mathbf{x}) &= 0, & \mathbf{x} \in \Omega, \\ u(\mathbf{x}) &= f(\mathbf{x}), & \mathbf{x} \in \partial\Omega.\end{aligned}\tag{1}$$

The solution at point \mathbf{x} can be represented probabilistically as the average over all the boundary values, $X^{\mathbf{x}}(\tau_{\partial\Omega})$, of Brownian motion starting at \mathbf{x} . The time, $\tau_{\partial\Omega}$, when the Brownian particle first strikes the boundary is called the first-passage time, and the place where the Brownian particle first strikes the boundary, $X^{\mathbf{x}}(\tau_{\partial\Omega})$, is called the first-passage location. Specifically, the probabilistic solution, $u(\mathbf{x})$, to (1) is given by

$$u(\mathbf{x}) = E^{\mathbf{x}}[f(X^{\mathbf{x}}(\tau_{\partial\Omega}))].\tag{2}$$

The proof that this is the case is simple. Place a sphere centered at \mathbf{x} completely lying within Ω . Clearly, the particle will have to hit this sphere before hitting $\partial\Omega$. The probability

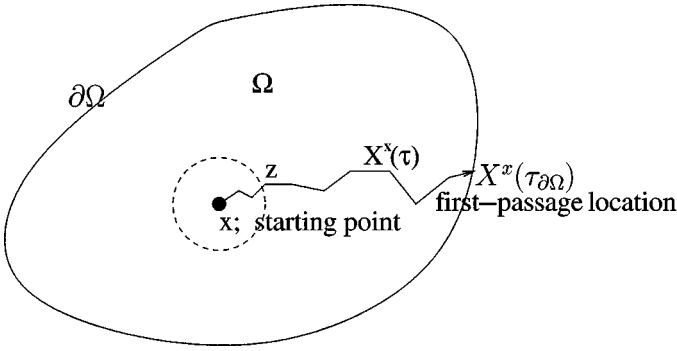


FIG. 1. Brownian motion which starts at \mathbf{x} and terminates at $X^{\mathbf{x}}(\tau_{\partial\Omega})$ on the boundary $\partial\Omega$ while passing through \mathbf{z} , a point on a sphere centered at \mathbf{x} .

distribution of \mathbf{z} , the FP position on the sphere, is clearly uniform due to the isotropic nature of Brownian motion. Now we continue the Brownian particle from \mathbf{z} until it hits the boundary. Here $X^{\mathbf{x}}(\tau_{\partial\Omega})$ is the first-passage location on the boundary, $\partial\Omega$ (see Fig. 1). Averaging over the first-passage boundary values of Brownian paths started at \mathbf{z} gives us $u(\mathbf{z})$. Since each trajectory starting at \mathbf{x} that hits $\partial\Omega$ must first hit the sphere with uniform probability, $u(\mathbf{x})$ must be the mean of the values of $u(\mathbf{z})$ over the sphere. Thus, $u(\mathbf{x})$ has the mean-value property and is harmonic, i.e., it obeys the Laplace equation [22]. If we then think of moving the starting point for our Brownian particles to the boundary, we clearly will, in the limit, have the first-passage location coincide with the limit of \mathbf{x} on the boundary. This argues that, in addition, $u(\mathbf{x})$ has the correct boundary values, and so it is the unique solution to (1).

The RHS of Eq. (2) can be interpreted as an average of the boundary values, $f(\mathbf{x})$, $\mathbf{x} \in \partial\Omega$ over $\partial\Omega$. The weighting factor in this average is the first-passage probability $p(\mathbf{x}, \mathbf{y})$ of a Brownian particle starting at \mathbf{x} hitting the boundary first at $\mathbf{y} = X^{\mathbf{x}}(\tau_{\partial\Omega}) \in \partial\Omega$. Thus, we can represent $u(\mathbf{x})$ as an integral over the boundary, $\partial\Omega$, via

$$u(\mathbf{x}) = \int_{\partial\Omega} p(\mathbf{x}, \mathbf{y}) f(\mathbf{y}) d\mathbf{y}. \quad (3)$$

However, there is another representation of the solution of the Dirichlet problem for the Laplace equation in terms of an integral over the boundary. This is provided by means of the Green's function, $G(\mathbf{x}, \mathbf{y})$ [23],

$$u(\mathbf{x}) = \int_{\partial\Omega} \frac{\partial G(\mathbf{x}, \mathbf{y})}{\partial \mathbf{n}} f(\mathbf{y}) d\mathbf{y}. \quad (4)$$

The normal derivative of the Green's function on $\partial\Omega$ is what we refer to as the “surface Green's function” for the domain Ω . Thus, the surface Green's function for a domain, Ω , must be *identical* to the first-passage probability distribution for that same domain: $p(\mathbf{x}, \mathbf{y}) = \partial G(\mathbf{x}, \mathbf{y})/\partial \mathbf{n}$.

Since the Laplace equation describes the electrical potential outside regions containing charges, one can also translate the probabilistic interpretation of the Laplace equation into the language of electrostatics [4, 20]. Thus, a point source of Brownian (diffusing) particles becomes a point charge; the “first-passage” (FP) surface becomes an ideal conductor,

the first-passage distribution on the FP surface becomes a charge distribution, the surface Green's function becomes the normal derivative of electrostatic potential, and the interface between different media becomes a dielectric interface.

For computational reasons, the ST method is limited at present to Green's functions that have three dimensionless parameters (or less) for arguments: two parameters (α, β) that define the geometry of the FP surface, and one parameter that defines the FP position in the geometry. In the applications treated here, the FP surface is a portion of a sphere and has azimuthal symmetry. Thus, the polar angle θ suffices to determine the FP position.

For each set of values of the geometrical parameters defined on a 2D grid, the value of $\cos \theta$ is binned, i.e., tabulated for a large number of trajectories. The simulation data provide a discrete approximation to the distribution

$$P(\alpha, \beta, \cos \theta) d\alpha d\beta d(\cos \theta). \quad (5)$$

This is the probability distribution associated with a Brownian particle making FP at a polar angle θ in the fixed geometry characterized by the two parameters (α, β). We next form the normalized distribution,

$$p(\alpha, \beta, \cos \theta) = \frac{1}{Z_n} \int_{-1}^{\cos \theta} P(\alpha, \beta, \cos \theta) d\alpha d\beta d(\cos \theta), \quad (6)$$

where Z_n is a normalizing factor. As a function of $\cos \theta$, the normalized distribution varies smoothly and monotonically between zero and unity. Thus, it can be inverted to give the function

$$\cos \theta(\alpha, \beta, p). \quad (7)$$

To sample this distribution, we choose a random number η uniformly in the interval $[0, 1)$, set $p = \eta$ in this function, and obtain a value of $\cos \theta$ via interpolation.

We now consider two basic Laplacian Green's functions that are useful when the particles are diffusing outside one or more spherical regions. (These Green's functions, of course, would not be "basic" for other geometries; one would need to generate other basic Green's functions for other geometries.)

We calculate and tabulate the Green's function for a point source located on the surface of a reflecting sphere and surrounded by an absorbing sphere (see the bold curves in Fig. 2); this Green's function allows a diffusing particle to leave a reflecting surface. In particular, we solve the Poisson equation

$$\Delta u(\mathbf{x}, \mathbf{x}_0) = \delta(\mathbf{x} - \mathbf{x}_0), \quad (8)$$

with the boundary conditions

$$\mathbf{n}(\mathbf{x}) \cdot \nabla u(\mathbf{x}, \mathbf{x}_0) = 0, \quad \mathbf{x} \in \partial\Omega_1, \quad (9)$$

$$u(\mathbf{x}, \mathbf{x}_0) = 0, \quad \mathbf{x} \in \partial\Omega_2. \quad (10)$$

Here, $\mathbf{n}(\mathbf{x}) \cdot \nabla u(\mathbf{x}, \mathbf{x}_0)$ is the probability density associated with hitting the vicinity of \mathbf{x} on the absorbing spherical surface for the first time when the Brownian particle starts from \mathbf{x}_0 . Here, $\mathbf{n}(\mathbf{x})$ is the normal vector at the surface point x .

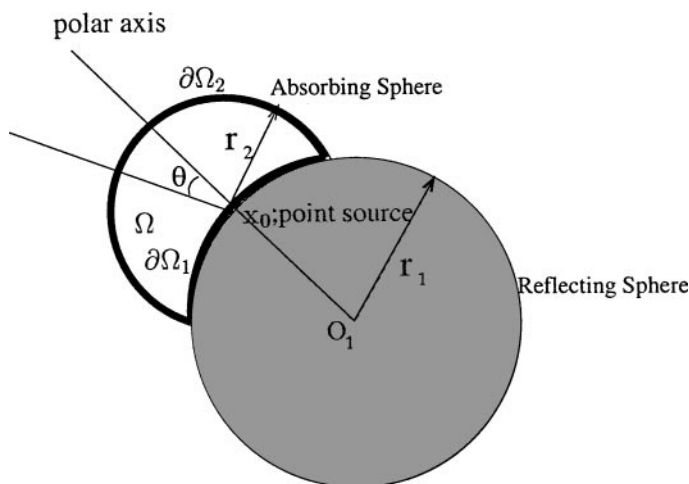


FIG. 2. The first-passage surface (bold curves) for a Brownian particle, located at point x_0 on a reflecting sphere of radius r_1 , to reach an absorbing FP surface $\partial\Omega_2$ of radius r_2 .

The tabulation (see tabulation 1 in Table I) has two parameters: the ratio $X = r_2/r_1$ of the radii, r_1 and r_2 , respectively, of the reflecting and the absorbing spheres; and the variable $Y = 1 - \cos \theta$, where θ is the polar angle giving the location on the absorbing sphere where FP occurs. Here, we use a polar coordinate system with the line connecting the two sphere centers as polar axis; we also exploit the azimuthal symmetry of this Green's function. The variable X ranges from 0 to 2 with step size of 0.02; for each value of X , Y ranges from 0 to $(1 - \cos \theta_{\max})$, where the angle, θ_{\max} , defined to be the largest angle for which the FP position is on the reflecting sphere, is determined by geometrical considerations (see Fig. 3):

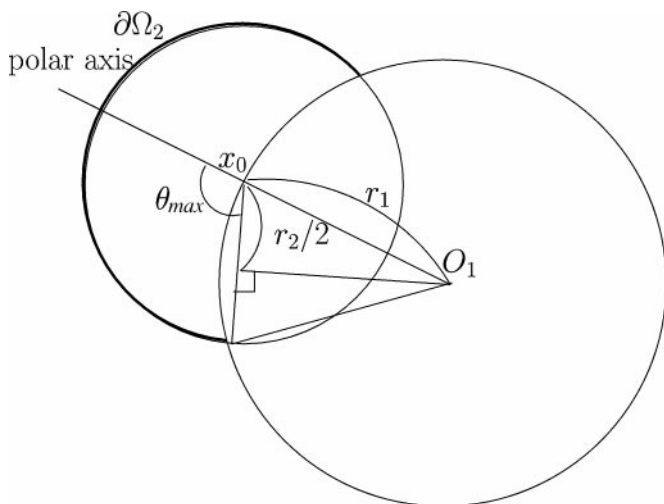


FIG. 3. The geometrical consideration for the calculation of $\cos \theta_{\max}$ in the first-passage surface for a Brownian particle, located at point x_0 on a reflecting sphere of radius r_1 , to reach an absorbing FP surface $\partial\Omega_2$ of radius r_2 .

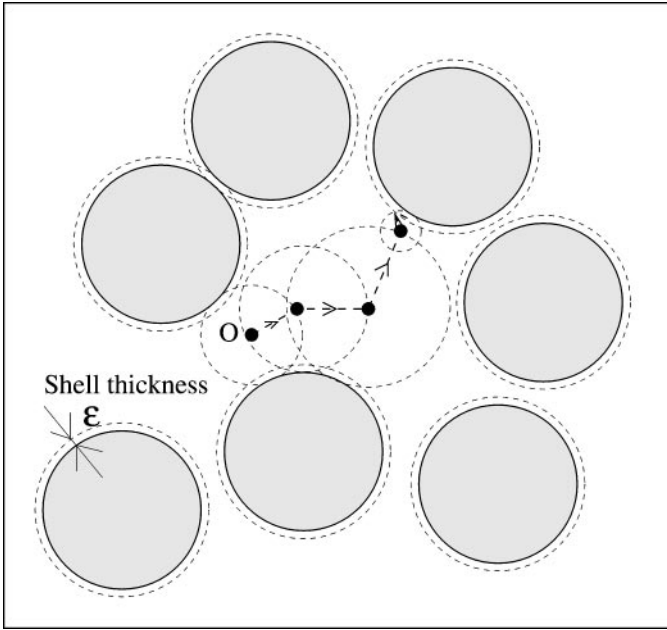


FIG. 4. A two-dimensional schematic representation of a Brownian trajectory using WOS algorithm. If the diffusing particle reaches the ϵ -layer, it is taken to be absorbed.

$$\cos \theta_{\max} = -\frac{r_2}{2r_1}. \quad (11)$$

For the limiting case of $X = 0$, we use a uniform FP probability density over $\partial\Omega_2$: in this limit, the interface to the reflecting sphere is flat and the problem can be solved analytically.

The simulation uses the WOS algorithm. The Brownian particle is initiated at the point source, x_0 . The FP surface consists of the portion of reflecting spherical surface contained within the FP sphere together with the portion of the FP sphere that is outside the reflecting spherical surface (see the bold curves in Fig. 2). The Brownian particle makes FP jumps using WOS until it lands within a distance ϵ of at least one point on the absorbing surface, $\partial\Omega_2$ (see Fig. 4). When this happens, the Brownian particle is taken to be absorbed on the portion of the FP surface.

As described in the Introduction, we have a standard procedure to convert simulation data into tabulation data, i.e., into data that can be directly sampled to provide the FP position.

At the same time, the average absorption time, i.e., the average lifetime of a Brownian particle, is tabulated (tabulation 2 in Table I). For the mathematical formulation, we start with the Feynman–Kac path-integral representation for solving the Dirichlet problem for Poisson’s equation:

$$\Delta u(\mathbf{x}) = q(\mathbf{x}), \quad \mathbf{x} \in \Omega \quad (12)$$

$$u(\mathbf{x}) = 0, \quad \mathbf{x} \in \partial\Omega. \quad (13)$$

The solution to this problem, given in the form of the path-integral with respect to standard

Brownian motion $X^x(t)$, is as follows [21, 24]:

$$u(\mathbf{x}) = E \left[- \int_0^{\tau_{\partial\Omega}} q(X^x(t)) dt \right]. \tag{14}$$

Here $\tau_{\partial\Omega}$ is the first-passage time of a Brownian particle starting at \mathbf{x} . We can see that when $q(\mathbf{x}) = -1$, $u(\mathbf{x}) = E[\int_0^{\tau_{\partial\Omega}} dt] = E[\tau_{\partial\Omega}]$. Thus, the mathematical formulation is a Dirichlet boundary problem for the Poisson equation with a constant source [25, 15],

$$\Delta u(\mathbf{x}) = -1, \quad \mathbf{x} \in \Omega, \tag{15}$$

and with the boundary conditions

$$u(\mathbf{x}) = 0, \quad \mathbf{x} \in \partial\Omega. \tag{16}$$

The average time, τ , required for a Brownian particle to first hit the surface of a sphere is given by $\tau = r^2/(6D)$, where r is the radius of the sphere and D the diffusion coefficient [26]. The average absorption time for a Brownian particle is given by the sum of this expression over all FP spheres used to construct the absorbed walk:

$$E[\tau_{\partial\Omega}] = E \left[\sum_i^N \frac{r_i^2}{6D} \right]. \tag{17}$$

Here, N is the number of WOS steps needed for the Brownian trajectory and r_i is the i th WOS radius.

The errors involved in these tabulations are the following: the absorption ϵ -shell approximation (described below), the assumption of uniform probability density when the radius of the restarting WOS FP surface is much smaller than that of the reflecting sphere, the statistical sampling error, and the error associated with the interpolation. The ϵ -shell error

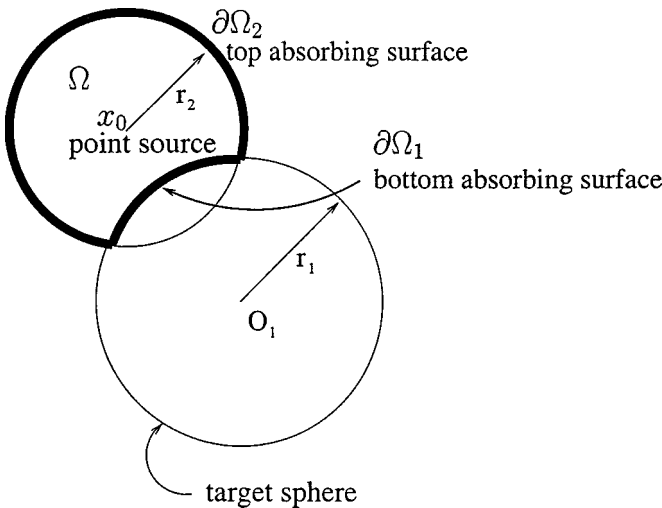


FIG. 5. The first-passage surface (bold curves) for a Brownian particle, initiating at the center x_0 of an absorbing sphere of radius r_2 and making FP either on that sphere $\partial\Omega_2$ or on the included portion $\partial\Omega_1$ of a second absorbing sphere of radius r_1 .

TABLE I
Summary of Our Four Tabulations

Tabulation	Description
Tabulation 1	Surface Green's function for Fig. 2 FP surface
Tabulation 2	Average hitting time for Fig. 2 FP surface
Tabulation 3	Surface Green's function for Fig. 5 FP surface
Tabulation 4	Average hitting time for Fig. 5 FP surface

can be made always less than the statistical error [13, 14]. We use $\epsilon = 10^{-4}r_1$ and 10^6 trajectories for each r_2/r_1 ratio. We do not estimate the error arising from interpolation or the assumption of uniform probability density over the restarting WOS FP surface.

Next, we calculate and tabulate the Green's function for a point source in the center of an absorbing sphere that intersects another absorbing sphere. This Green's function (and others like it) are the basis of the GFFP method: they allow a FP jump directly to an absorbing surface (see Fig. 5). The FP surface is the top and bottom absorbing surface enclosing the point source; it includes the portion of FP sphere outside the target sphere, $\partial\Omega_2$, and the portion of the target sphere contained in the FP sphere, $\partial\Omega_1$ (see the bold curves in Fig. 5). The Poisson problem to be solved in this case is the same as that defined by Eqs. (8)–(10), except that the reflecting boundary condition, Eq. (9), is replaced by the absorbing boundary condition

$$u(x, x_0) = 0, \quad x \in \partial\Omega_1. \quad (18)$$

For this problem, analytic solutions are known [27, 28] and have been used to do GFFP calculations by one of us [11] (see tabulation 3 in Table I). However, for rapid and accurate conductivity calculations we need to perform a high-order tabulation of this function; we need to tabulate the average absorption time as well (see tabulation 4 in Table I). Each of these tabulations has two parameters: the ratio X of the radii r_1 and r_2 of the two intersecting spheres and the dimensionless distance Z from the center of the intersecting sphere to the surface of the other sphere divided by r_1 . Both variables range from 0.02 to 1.00 with step size 0.02. For the limiting case of $X = r_2/r_1 = 0$, the average absorption time is 0.

In our simulation, the Brownian particle starts from the point source. We use the WOS algorithm until the Brownian particle is absorbed on the FP surface. We calculate the average FP time by accumulating the radius square of WOS as in the previous case. We use $\epsilon = 10^{-4}r_1$ and 10^6 trajectories for each r_2/r_1 ratio.

We summarize our tabulations in Table I.

3. APPLICATION OF THE ST METHOD TO THREE BASIC DIFFUSION-LIMITED APPLICATIONS

In this section, we use the ST Green's functions to solve three basic classes of diffusion problems: the Solc–Stockmayer model with zero potential, the mean trapping rate of a diffusing particle in a domain of nonoverlapping spherical traps, and the effective conductivity for perfectly insulating, nonoverlapping spherical inclusions in a matrix of conductivity σ_1 . This class of problems will test all four tabulated Green's functions described in Section 2.

First, we calculate the reaction rate constant of the Solc–Stockmayer model without potential, a basic model for diffusion-limited protein–ligand binding. A model protein molecule

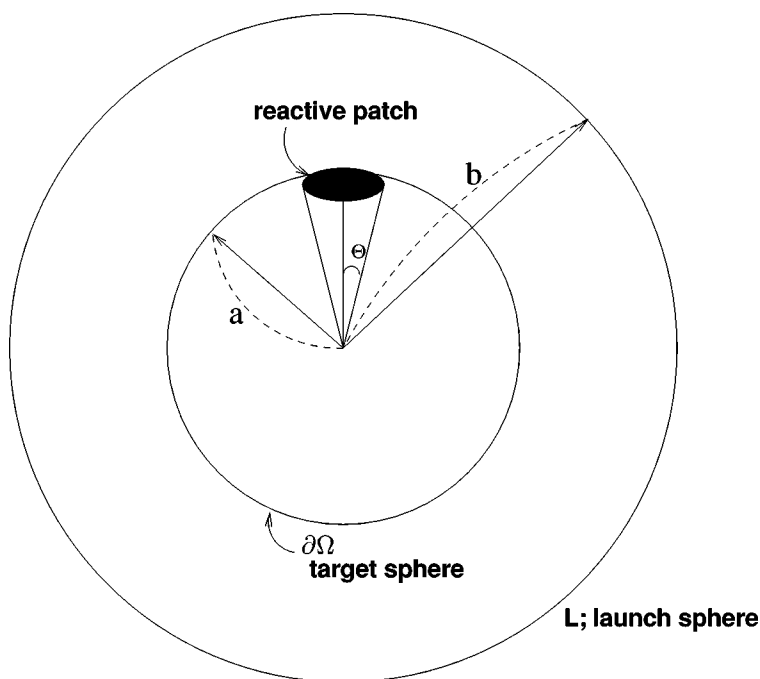


FIG. 6. A schematic diagram that illustrates the simple Solc-Stockmayer model for diffusion-limited protein-ligand binding. L is the launch sphere with radius b where diffusing ligand is launched with uniform probability distribution and $\partial\Omega$ is the surface of a protein of radius $a = 1.0$ with a circular reactive patch with angle Θ . The reactive patch is absorbing and the rest of the protein reflecting.

is a sphere with a circular patch on its surface producing irreversible binding upon contact with a diffusing ligand; the remainder of the spherical surface is nonreactive, i.e., reflecting. Ligand molecules are idealized as noninteracting point-like diffusing particles.

For maximum efficiency, the basic methods used here for the calculation of the reaction rate constant are refinements of the capture probability method [29] (see Fig. 6). The reaction rate constant κ we wish to compute is given by [6]

$$\frac{\kappa}{4\pi Da} = b\beta, \quad (19)$$

where β is the fraction of diffusing ligands from the launch sphere that are absorbed on the reactive patch, and D is the diffusion coefficient. Each diffusing ligand initiates on the launch sphere of radius b surrounding the target sphere of radius a , i.e., the protein model, at a position chosen at random (see Fig. 6). It makes FP jumps (as described below) until it either reaches the reactive patch on the target sphere (shaded area in Fig. 6) or goes to infinity.

In this problem there are novel aspects. If the diffusing ligand jumps to a point on the reflecting portion of the target sphere, it uses the first Green's function described in Section 2 to leave the surface (see Fig. 2). In this case, the FP sphere must not be large enough to intersect the boundary of the absorbing patch. When the diffusing ligand jumps to the reactive patch, it is absorbed.

We describe two methods for this calculation. The first method tests only tabulation 1 and the second tabulations 1 and 3 (we validate tabulation 1 through the first method and tabulation 3 through the second method).

In the first method, a diffusing ligand is initially placed at a randomly determined position on the surface of the launch sphere. Instead of using the WOS or GFFP method, we use a known probability (Eq. (20)) to decide whether the diffusing ligand goes to the target sphere or to infinity from the randomly determined position on the surface of the launch sphere. When it is determined to land on the target sphere, we use the replacement distribution function (Eq. (21)). The probability that the ligand escapes to infinity from the surface of the launch sphere [7] is given by

$$P_{\text{esp}} = 1 - \frac{a}{b} = 1 - \alpha. \quad (20)$$

Here b is the launch sphere radius and a is the target sphere radius. If the ligand lands on the target sphere, it will land at a position (θ, ϕ) sampled by the replacement distribution density function [7]

$$\omega(\theta, \phi) = \frac{1 - \alpha^2}{4\pi[1 - 2\alpha \cos \theta + \alpha^2]^{3/2}}. \quad (21)$$

Here, (θ, ϕ) are defined with respect to the polar axis that joins the old position to the target sphere center and α is a/b . This distribution function has no ϕ dependence due to symmetry. If the diffusing ligand lands on the absorbing patch, it is absorbed. If not, we construct an intersecting first-passage sphere centered on the absorption point just large enough to touch the patch boundary. Using the tabulated Green's function (tabulation 1), we find the next first-passage point. The probability that the diffusing ligand escapes to infinity from the first-passage point without absorbing on the target sphere is given by [7]

$$P_{\text{esp}} = 1 - \frac{a}{r_0}. \quad (22)$$

Here r_0 is the radial position of the diffusing ligand. If the ligand lands on the target sphere instead of going to infinity, the replacement distribution density function with $\alpha = a/r_0$ is used to determine the new position on the target sphere. This procedure iterates until the ligand either reaches the reactive patch on the target sphere or goes to infinity.

The simulation results with 10^6 and 10^9 trajectories are shown in Table II. We obtain three digits of accuracy. This is consistent with the accuracy of our Green's function tabulations. We can reproduce the results using only WOS without tabulation 1, but the computation

TABLE II
Reaction Rate Constant $\kappa/(4\pi Da)$ for the Solc-Stockmayer
Model without Potential^a

Angle (Θ)	Exact	Simulation (10^6)	Simulation (10^9)
10	0.64925E - 01	0.64516E - 01	0.65074048E - 01
20	0.14179E + 00	0.14159E + 00	0.14196463E + 00
30	0.22628E + 00	0.22673E + 00	0.22642986E + 00

^a This is the first of the two methods we provide for this problem in Section 3. It uses analytic replacement distribution function and tabulation 1. It is our most efficient method. The left-hand column gives analytic results by the method of dual series relations [30]. The other two columns give our simulation results with 10^6 and 10^9 diffusing ligands, respectively. They are accurate up to three digits.

time is substantially greater. To compare with our simulation results, the exact values are obtained by the method of dual series relations [30].

To increase the accuracy of the calculations, we can increase the number of trajectories for each r_2/r_1 ratio to reduce the statistical error, keep the boundary error less than the statistical error [13, 14], and use a smaller radius for the FP sphere used to leave the reflecting sphere in the tabulation 1.

Next, we describe our second method for addressing this problem. The Green's function for this problem (see Fig. 5) samples the FP position on both the upper and the lower absorbing surface. The former has been carefully tested [11, 18]; the latter has not. In this work, we refine the accuracy of the FP distribution on the lower absorbing surface. (In a separate paper [19], we have shown that this refinement in accuracy and other algorithmic improvements in our permeability estimation methods [18] improve our permeability estimates quite substantially, especially at low porosities.) Because the first method has already been described, we discuss in detail only those aspects of the second method that are different. The diffusing ligand propagates by a series of FP jumps (see Fig. 7), each

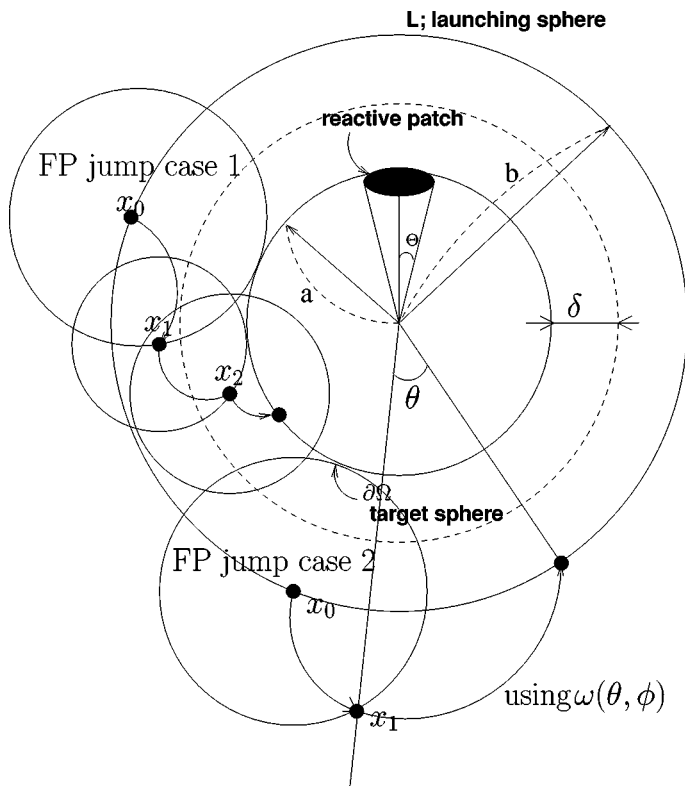


FIG. 7. A schematic diagram that illustrates FP jumps using GFFP in the simple Solc–Stockmayer model for diffusion-limited protein–ligand binding. L is the launch sphere with radius b where diffusing ligand is launched with uniform probability distribution and $\partial\Omega$ is the surface of a protein of radius $a = 1.0$ with a circular reactive patch with angle Θ . The reactive patch is absorbing and the rest of the protein reflecting. In FP jump case 1, the figure shows δ -boundary layer usage; when the diffusing particle reaches inside the δ -boundary layer, it begins to intersect the target sphere; in FP jump case 2, the figure shows the usage of the replacement distribution density function when the first jump from the launch sphere is outside the launch sphere and the probability decides that the diffusing particle goes back to the launch sphere.

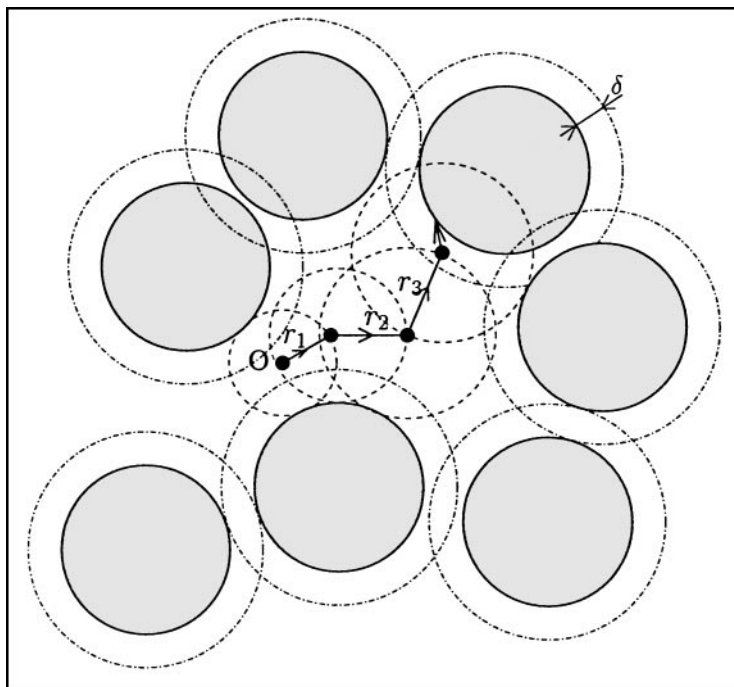


FIG. 8. A two-dimensional schematic representation of a Brownian trajectory using both the WOS algorithm (r_1 to r_3) and the GFFP algorithm (the final step). The solid circles are FP boundaries and absorbing. We use a δ -boundary layer as a criterion such that WOS is used outside the δ -boundary layer and GFFP in the δ -boundary layer.

proceeding from the starting point (x_0 in our notation) to a point on its FP surface. The surface point to which it jumps is determined by sampling the tabulated distribution function associated with the appropriate Laplacian Green's function, obtained as described in the previous section. For efficiency, the FP volume is chosen to be a sphere with uniform FP probability until the diffusing ligand gets into the δ -boundary layer; then the FP volume is chosen to be a sphere that intersects the target sphere. (Throughout this paper, we use the δ -boundary layer as a criterion such that WOS is used outside the δ -boundary layer and GFFP in the δ -boundary layer, because GFFP is more efficient when the Brownian particle gets close to the target; see Fig. 8.) Notice that this δ -boundary layer is different from the ϵ -shell in WOS (see Fig. 4).

Table III shows the simulation results with 10^6 trajectories. These are accurate up to three digits also.

We compare the CPU time of the ST algorithm with that of the WOS algorithm in Figs. 9 and 10. In the WOS algorithm, CPU time depends on the ϵ -shell thickness and the ST algorithm on the δ -boundary layer. The value of $\epsilon = 10^{-3}a$ in the WOS method approximately corresponds to the optimal case of ST. Considering that for the accuracy of up to three digits in the WOS algorithm we need approximately $\epsilon = 10^{-6}a$, the ST algorithm is two times faster when we use the optimal case of ST (in Fig. 9, the running time of the WOS algorithm at $\epsilon = 10^{-6}a$ is approximately 2600 s while the running time of the ST algorithm at $\delta = 0.1a$ is approximately 1350 s in Fig. 10). The ST results can be reproduced using only WOS without tabulations 1 and 3, but the computation time is much greater.

TABLE III
Reaction Rate Constant $\kappa/(4\pi Da)$ for the Solc–Stockmayer
Model without Potential^a with $\epsilon = 0$ and $\delta = 0.3a$

Angle (Θ)	Exact	Simulation (10^6)
10	$0.64925E - 01$	$0.64975E - 01$
20	$0.14179E + 00$	$0.14244E + 00$
30	$0.22628E + 00$	$0.22697E + 00$

^a This is the second of the two methods we provide for this problem in Section 3. It uses tabulations 1 and 3, the tabulated Green's functions new to the present work. Here, ϵ is the absorption shell thickness and δ is the distance from the surface of the sphere within which the first-passage sphere begins to intersect the target.

Next, we simulate the diffusion-limited trapping rate in a system of noninteracting diffusing particles in a volume containing nonoverlapping spherical traps (see Fig. 8). This will test tabulation 4 (we use tabulations 3 and 4, but we validated tabulation 3 in the previous Solc–Stockmayer problem). The trapping rate is obtained as the inverse of the average survival time [31]. The average survival time is given by

$$E[\tau] = E \left[\sum_i^{N_w} \frac{r_i^2}{6D} + \sum_j^{N_g} \tau_j \right], \quad (23)$$

when we choose starting points randomly inside the void space. Here, N_w is the number of WOS steps during the Brownian trajectory, r_i the i th WOS radius, N_g the number of GFFP steps during the Brownian trajectory, and τ_j the sampled time using tabulation 4 for the j th GFFP step. The mean trapping rate simulations are performed on systems

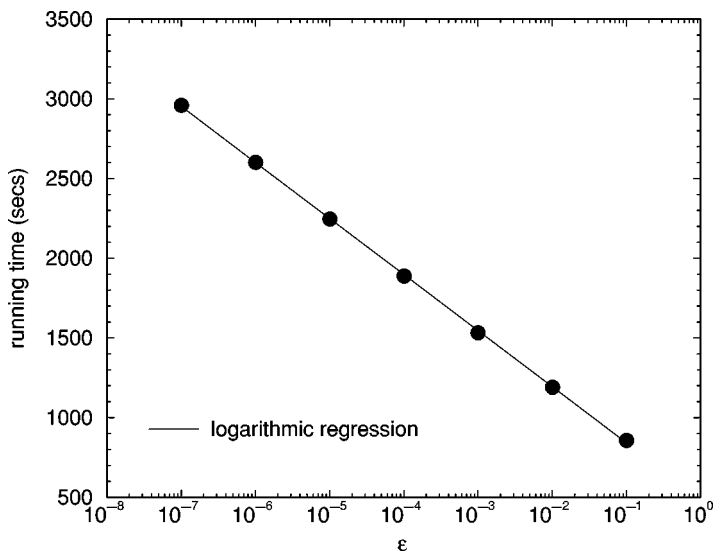


FIG. 9. CPU time required to calculate the reaction rate constant for the Solc–Stockmayer model without potential using only WOS with $\Theta = 10^0, 10^7$ trajectories, $\delta = 0$, $a = 1.0$, and $b = 2.0$ on a 500-MHz Pentium III work station. It shows the expected relation for WOS:CPU time $\sim \ln(\epsilon)$.

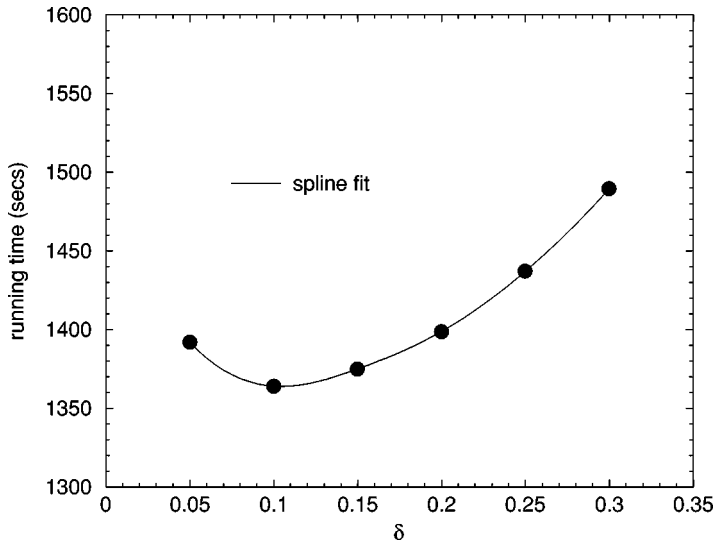


FIG. 10. CPU time required to calculate the reaction rate constant for the Solc–Stockmayer model without potential using GFFP with $\Theta = 10^6$, 10^7 trajectories, $\epsilon = 0$, $a = 1.0$, and $b = 2.0$ on a 500-MHz Pentium III workstation. It shows an optimal δ around $\delta = 0.1a$.

consisting of 95–668 nonoverlapping spheres with radius $a = 1.0$, depending on the sink volume fraction ϕ_2 . The results of ST algorithm are compared with those of Zheng–Chiew simulations [31] using WOS in Fig. 11. At low-volume fractions, there are some deviations due to sampling fluctuation. We consider 10 realizations, each constructed by using random sequential addition [31, 32], and simulate 10^5 diffusing particles per realization.

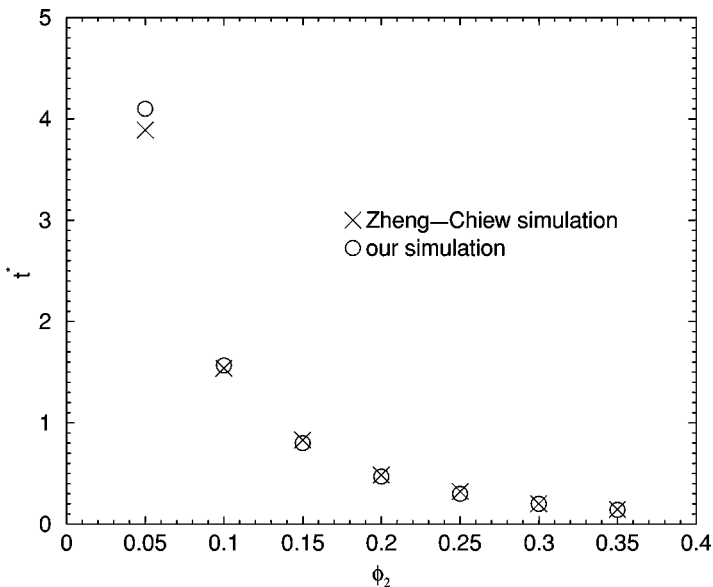


FIG. 11. Average survival time as a function of the sink volume fraction ϕ_2 for nonoverlapping impenetrable spheres. The crosses represent the simulation data from Zheng–Chiew calculation and the circles our simulation data. At low-volume fractions, there are some deviations due to sampling fluctuation.

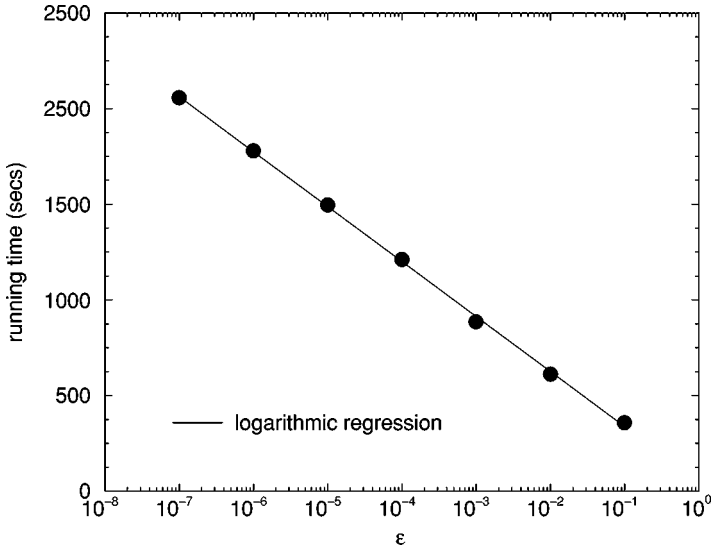


FIG. 12. CPU time required to calculate the mean trapping rate for nonoverlapping impenetrable spheres using only WOS with $\phi_2 = 0.05$, 10^6 trajectories, $\delta = 0$, $a = 1.0$, and 95 nonoverlapping impenetrable spheres on a 500-MHz Pentium III work station. It shows the expected relation for WOS:CPU time $\sim \ln(\epsilon)$.

The CPU time of the ST algorithm is compared with that of the WOS algorithm in Figs. 12 and 13. As the previous case, in the WOS algorithm, CPU time depends on the ϵ -shell thickness and the ST algorithm on the δ -boundary layer. Approximately $\epsilon = 10^{-3}a$ in the WOS method corresponds to the optimal case of ST. Considering that for the accuracy of up to three digits in the WOS algorithm we need approximately $\epsilon = 10^{-6}a$, the ST algorithm is one and half times faster when we use the optimal case of ST (in Fig. 12, the

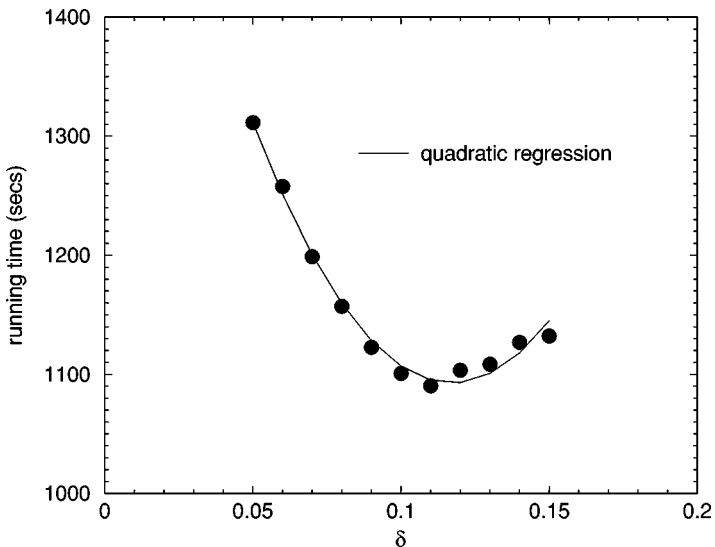


FIG. 13. CPU time required to calculate the mean trapping rate for nonoverlapping impenetrable spheres using GFFP with $\phi_2 = 0.05$, 10^6 trajectories, $\epsilon = 0$, $a = 1.0$, and 95 nonoverlapping impenetrable spheres on a 500-MHz Pentium III work station. It shows an optimal δ around $\delta = 0.12a$.

running time of the WOS algorithm at $\epsilon = 10^{-6}a$ is approximately 1600 s while the running time of the ST algorithm at $\delta = 0.11a$ is approximately 1100 s in Fig. 13).

Finally, we simulate the bulk (or effective) conductivity of a two-phase system composed of nonoverlapping insulating spherical inclusions dispersed in a conducting matrix with a conductivity σ_1 . This provides a nontrivial test of tabulation 2 (we use all tabulations, but we validated all the others except 2 in the previous Solc–Stockmayer model and trapping rate simulations). The effective conductivity, σ_e , of general two-phase media can be obtained by using the Einstein relation between conductivity and diffusion [17]:

$$\sigma_e = \frac{X^2}{6\tau_e(X)}. \quad (24)$$

Here, $\tau_e(X)$ is the total mean time associated with the total mean-square displacement X^2 ,

$$\tau_e(X) = E \left[\sum_i^{N_w} \frac{r_i^2}{6D} + \sum_j^{N_g} \tau_j \right], \quad (25)$$

when we choose starting points randomly inside the void space. Here, N_w is the number of WOS steps during the Brownian trajectory, r_i the i th WOS radius, N_g the number of GFFP steps during the Brownian trajectory, and τ_j the sampled time using tabulations 2 and 4 for the j th GFFP step. In our simulations, we choose X^2 for the conductivity calculation. For efficiency, we use WOS until the diffusing particle reaches the δ -boundary of any nearby reflecting sphere. We then use the nontrivial Green's function shown in Fig. 5 (r_2 should be small enough that the sphere of radius r_2 does not intersect the second nearest inclusion sphere). Here we use $\delta = 0.3a$, where a is the radius of the reflecting spheres (we chose this value of δ at random because there was very little information available on optimizing the choice of δ for random media problems). If the diffusing particle makes an FP jump on the reflecting sphere, we use the nontrivial Green's function shown in Fig. 2 to leave the reflecting sphere. We calculate the mean FP time for a diffusing particle by accumulating the mean FP time for each jump. If the FP surface for a jump is a sphere, this FP time is proportional to the radius squared; if the FP surface is not spherical, we use the value from the FP time tabulation described in the previous section (tabulations 2 and 4). This illustrates the bootstrap nature of the ST method: here we use as a primitive tabulation obtained in a previous study. If a Green's function simulation, providing a FP position and a FP time for a particular FP surface geometry, has been performed once, there is no reason to ever do it again. We also repeated this set of simulations using the value $\delta = 0$, i.e., we used WOS only, until a diffusing particle jumped to within the distance ϵ of a reflecting sphere. It is then considered to be "absorbed" at the closest point on the sphere, and then leaves the reflecting sphere using the Green's function shown in Fig. 2.

The research by Kim and Torquato [17] is similar to this second method we described (using only WOS; i.e., $\delta = 0$). In their work, they use analytic solutions for both the absorption time and the probability that a diffusing particle "absorbed" on an interfacial surface will jump to a point outside that surface. But these authors do not use Green's function methods to sample the FP position. Thus, they use a very small FP sphere when leaving an interfacial surface. Also, they assume that a diffusing particle making such a jump will land on a point on the normal to the interface, drawn at the point of departure; i.e., the jump will have $\theta = 0$ or $\theta = \pi$, in our terminology. This approximation is highly accurate in this

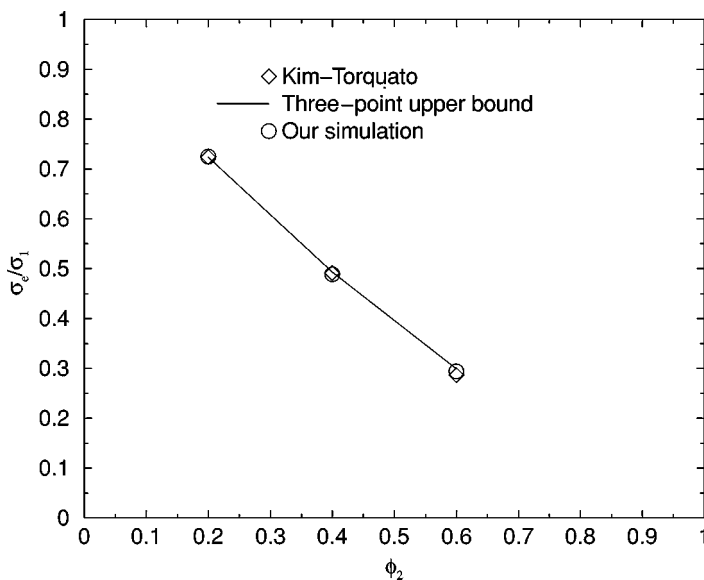


FIG. 14. Scaled effective conductivity σ_e/σ_1 of equilibrium distributions of nonoverlapping insulating spheres in a matrix of conductivity σ_1 with $\epsilon = 0.0001a$ and $\delta = 0$.

case for reasons which are not clear, but cannot be more efficient than our second method described above because it requires the FP radius for a jump leaving an interface to be small. In turn, our first method (using a nontrivial FP surface) described above is superior to the second method ($\delta = 0$ case).

Equilibrium configurations of nonoverlapping spheres are generated by the conventional Metropolis algorithm [17] with 128 spheres, where each sphere is moved 400 times. We considered 10 equilibrium realizations and 10^4 random walks per realization with dimensionless total mean square displacement (X^2/a^2) from 10 to 100 depending on volume fraction ϕ_2 . The simulation results are shown in Figs. 14 and 15.

Again, we compare the CPU time of the ST algorithm with that of the WOS algorithm in Figs. 16 and 17. In the WOS algorithm, CPU time depends on ϵ -shell thickness and the ST algorithm on δ -boundary layer. Here, $\epsilon = 10^{-1}a$ in the WOS method approximately corresponds to the optimal case of ST. Considering that for the accuracy of up to three digits in the WOS algorithm we need approximately $\epsilon = 10^{-6}a$, the ST algorithm is seven times faster when we use the optimal case of ST (in Fig. 16, the running time of the WOS algorithm at $\epsilon = 10^{-6}a$ is approximately 700 s while the running time of the ST algorithm at $\delta = 0.6a$ is approximately 100 s in Fig. 13).

4. COMPUTATIONAL EFFICIENCY OF THE ST METHOD

In this section, we discuss the issue of the efficiency of ST (and GFFP) methods compared with WOS methods. WOS is efficient until one gets very close to an absorbing surface. (In GFFP methods all surfaces are “absorbing,” in the sense that they furnish natural boundaries to FP jumps i.e., the Brownian particle must stop upon contact with them. GFFP methods then use a surface Green’s function, such as that shown in Fig. 2, to sample a landing position

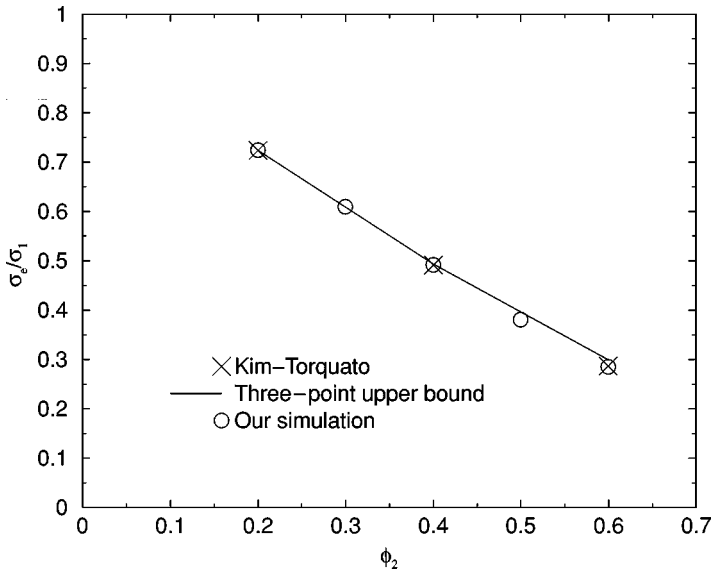


FIG. 15. Scaled effective conductivity σ_e/σ_1 of equilibrium distributions of nonoverlapping insulating spheres in a matrix of conductivity σ_1 with $\epsilon = 0$ and $\delta = 0.1a$.

for the next FP jump. Of course, if the surface is really absorbing, this is not necessary.) In random medium problems, Brownian particles are, on the average, very close to absorbing surfaces. Classical diffusion Monte Carlo methods do not yet have in place general theorems that relate the ϵ -shell to the accuracy that can be obtained in a Monte Carlo simulation. Generally, in WOS methods, the error from the ϵ -shell is made smaller than the statistical

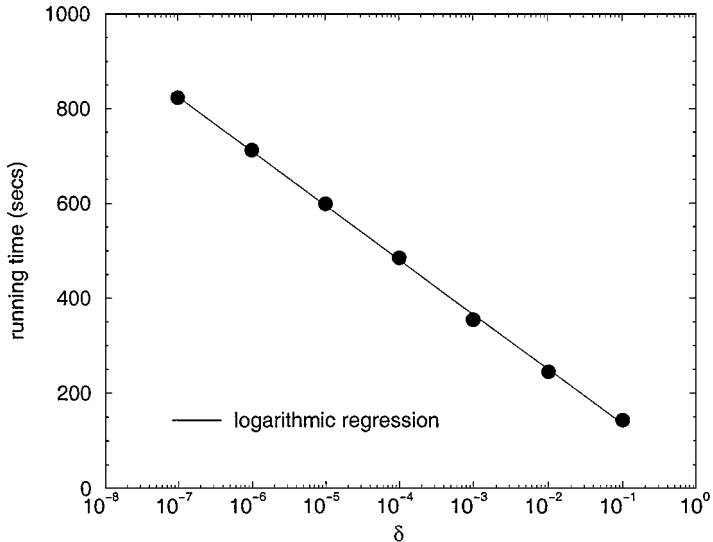


FIG. 16. CPU time required to calculate the effective conductivity of a system of nonoverlapping, insulating spherical inclusions dispersed randomly in a conducting matrix with sink volume fraction $\phi_2 = 0.2$. Here, we use WOS with mean diffusion path length $X^2/a^2 = 100$. We simulate 10^4 random walks on a 500-MHz Pentium III work station. The simulations show the expected relation for WOS: CPU time $\sim \ln(\epsilon)$.

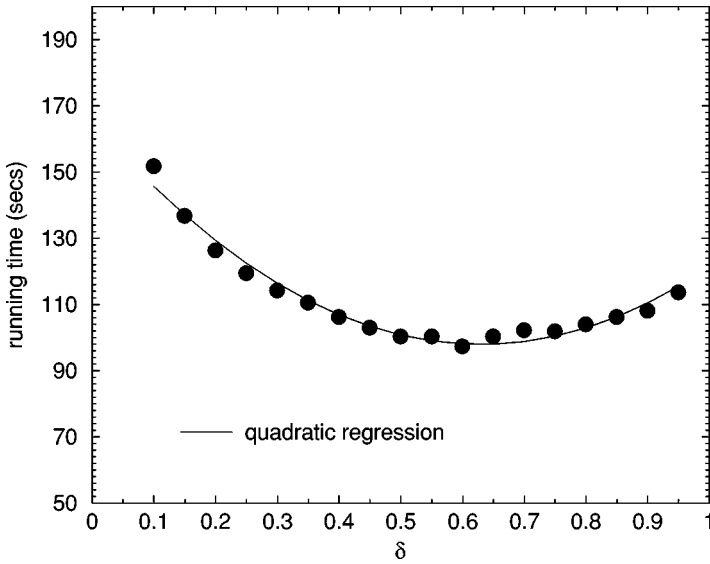


FIG. 17. CPU time required to calculate the effective conductivity of a system of nonoverlapping, insulating spherical inclusions dispersed randomly in a conducting matrix with sink volume fraction $\phi_2 = 0.2$. Here, we use GFPF with mean diffusion path length $X^2/a^2 = 100$. We simulate 10^4 random walks on a 500-MHz Pentium III work station. It shows an optimal δ around $\delta = 0.65a$.

error [13, 14]. For the same Brownian trajectory, the estimated difference between using ϵ and $\epsilon/10$ gives a measure of the error due to the ϵ -shell. By adjusting ϵ , we can make the error from the ϵ -shell less than the statistical error. This means that if we increase the number of Brownian particles to decrease the statistical error, we must consequently reduce ϵ and thus increase CPU time (the average number of FP jumps required for a Brownian particle to be absorbed in the ϵ -shell in WOS is $O(|\ln \epsilon|)$). This virtually guarantees that WOS methods will not be that useful for all problems that require accuracy beyond a preset limit. Generally, it is assumed that the accuracy attainable in a simulation in WOS is on the order of $\epsilon^{1/\gamma}$ as $\epsilon \rightarrow 0$ for some $\gamma > 0$ [33]. But very little data are available to quantify this claim. So we cannot yet provide thresholds of accuracy beyond which our method is the most efficient. This question is under investigation.

5. CONCLUSIONS AND FUTURE WORK

In this paper, we have developed an extension of our Green's function first-passage method that allows this method to be used on problems for which the Green's functions necessary to deal with a local interfacial surface cannot be obtained in analytic or quasi-analytic form. We test this simulation-tabulation method by applying it to three characteristic diffusion problems encountered in science and engineering. In all three cases, we reproduce numerically accurate solutions at substantially reduced computational cost. In essence, this method is able to do this because it allows a Brownian particle near an interface to sample the FP position even when the interface is not simple, and the FP radius is not small.

In particular, we show that, for each of the three problems we study, the ST method is the most efficient, provided that a sufficiently high level of accuracy is required. We show

explicitly that our method is more efficient than WOS, and by implication, any method that requires the use of small FP spheres close to an interface.

The methodological implications of this method for the study of this class of problems, namely Laplace boundary-value problems with complicated boundaries, are twofold. First, it is extremely inefficient for researchers pursuing the GFFP method to hoard Green's functions that they have calculated and tabulated. The best idea would be for one researcher to create a Web site where useful tabulated Green's functions can be stored and uploaded by other researchers. At present, we are making these Green's functions available at our group research Web page: <http://www.cs.fsu.edu/~mascagni/research>. Second, the central obstacle to the unlimited expansion of this research paradigm is the occurrence of FP configurations such that the number of independent geometrical parameters, together with the number of independent FP position parameters (like the polar angle θ), add up to 4 or more. A tabulated Green's function of three parameters, each parameter being tabulated at 200 discrete values, may not fit into cache memory in a modern computer; the same matrix of four dimensions will not fit into the cache memory. A limited solution to this problem is to allow the FP sphere radius, and the associated dimensionless parameter, to assume only a small number of values and then to use higher-order interpolation strategies. These matters are now under study.

ACKNOWLEDGMENTS

We give special thanks to Joe Hubbard, Kai Lai Chung, Karl K. Sabelfeld, and Henry P. McKean for their useful discussions. Also, we are especially grateful to Thomas Booth for a thorough reading of this manuscript.

REFERENCES

1. K. K. Sabelfeld, *Monte Carlo Methods in Boundary Value Problems* (Springer-Verlag, Berlin, 1991).
2. B. L. Hammond, W. A. Lester Jr., and P. J. Reynolds, *Monte Carlo Methods in Ab Initio Quantum Chemistry* (World Scientific, Singapore, 1994).
3. K. K. Sabelfeld, Integral and probabilistic representations for systems of elliptic equations, *Math. Comput. Model.* **23**, 111 (1996).
4. V. Zaloj and N. Agmon, Electrostatics by Brownian dynamics: Solving the Poisson equation near dielectric interfaces, *Chem. Phys. Lett.* **270**, 476 (1997).
5. S. H. Northrup, S. A. Allison, and J. A. McCammon, Brownian dynamics simulation of diffusion-influenced bimolecular reactions, *J. Chem. Phys.* **80**(4), 1517 (1984).
6. H.-X. Zhou, On the calculation of diffusive reaction rates using Brownian dynamics simulations, *J. Chem. Phys.* **92**(5), 3092 (1990).
7. B. A. Luty, J. A. McCammon, and H.-X. Zhou, Diffusive reaction rates from Brownian dynamics simulations: Replacing the outer cutoff surface by an analytical treatment, *J. Chem. Phys.* **97**, 5682 (1992).
8. J. Antosiewicz, J. A. McCammon, S. T. Wlodek, and M. K. Gilson, Simulation of charge-mutant acetylcholinesterases, *Biochemistry* **34**, 4211 (1995).
9. L. M. Schwartz, N. Martys, D. P. Bentz, E. J. Garboczi, and S. Torquato, Cross-property relations and permeability estimation in model porous media, *Phys. Rev. E* **48**, 4584 (1993).
10. C.-O. Hwang, J. A. Given, and M. Mascagni, A new fluid permeability estimation, *Proceedings of the First Southern Symposium on Computing*, available at [http://www.cs.fsu.edu/cmi/fsc98_html/processed/Hwang-et al \(1999\)](http://www.cs.fsu.edu/cmi/fsc98_html/processed/Hwang-et al (1999)).
11. J. A. Given, J. B. Hubbard, and J. F. Douglas, A first-passage algorithm for the hydrodynamic friction and diffusion-limited reaction rate of macromolecules, *J. Chem. Phys.* **106**(9), 3721 (1997).
12. M. E. Müller, Some continuous Monte Carlo methods for the Dirichlet problem, *Ann. Math. Stat.* **27**, 569 (1956).

13. T. E. Booth, Regional Monte Carlo solution of elliptic partial differential equations, *J. Comput. Phys.* **47**, 281 (1982).
14. T. E. Booth, Exact Monte Carlo solution of elliptic partial differential equations, *J. Comput. Phys.* **39**, 396 (1981).
15. S. Torquato, I.-C. Kim, and D. Cule, Effective conductivity, dielectric constant, and diffusion coefficient of digitized composite media via first-passage-time equations, *J. Appl. Phys.* **85**, 1560 (1999).
16. I. T. Dimov and T. V. Gurov, Estimates of the computational complexity of iterative Monte Carlo algorithm based on Green's function approach, *Math. Comput. Simulat.* **47**, 183 (1998).
17. I. C. Kim and S. Torquato, Effective conductivity of suspensions of hard spheres by Brownian motion simulation, *J. Appl. Phys.* **69**(4), 2280 (1991).
18. C.-O. Hwang, J. A. Given, and M. Mascagni, On the rapid calculation of permeability for porous media using Brownian motion paths, *Phys. Fluids A* **12**(7), 1699 (2000).
19. C.-O. Hwang, J. A. Given, and M. Mascagni, Rapid diffusion Monte Carlo algorithms for fluid dynamic permeability, *Monte Carlo Meth. Appl.* **7**(3–4), 213 (2001).
20. S. C. Port and C. J. Stone, *Brownian Motion and Classical Potential Theory* (Academic Press, New York, 1978).
21. M. Freidlin, *Functional Integration and Partial Differential Equations* (Princeton Univ. Press, Princeton, NJ, 1985).
22. F. John, *Partial Differential Equations* (Springer-Verlag, Berlin, Heidelberg, New York, 1982).
23. E. C. Zachmanoglou and D. W. Thoe, *Introduction to Partial Differential Equations with Applications* (Dover, New York, 1976).
24. K. L. Chung and Z. Zhao, *From Brownian Motion to Schrödinger's Equation* (Springer-Verlag, Berlin, 1995).
25. P. Hänggi, P. Talkner, and M. Borkovec, Reaction-rate theory: Fifty years after Kramers, *Rev. Mod. Phys.* **62**, 251 (1990).
26. S. Torquato and I. C. Kim, Efficient simulation technique to compute effective properties of heterogeneous media, *Appl. Phys. Lett.* **55**, 1847 (1989).
27. J. C. Maxwell, *A Treatise on Electricity and Magnetism* (Dover, New York, 1954), Vol. 1.
28. H. M. MacDonald, The electrical distribution on a conductor bounded by two spherical surfaces cutting at any angle, *Proceedings of the London Mathematical Society* **26**, 156 (1895).
29. H.-X. Zhou, Comparison of three Brownian-dynamics algorithms for calculating rate constants of diffusion-influenced reactions, *J. Chem. Phys.* **108**(19), 8139 (1998).
30. S. D. Traytak and M. Tachiya, Diffusion-controlled reaction rate to asymmetric reactants under Coulomb interaction, *J. Chem. Phys.* **102**(23), 9240 (1995).
31. L. H. Zheng and Y. C. Chiew, Computer simulation of diffusion-controlled reactions in dispersions of spherical sinks, *J. Chem. Phys.* **90**(1), 322 (1989).
32. B. Widom, Random sequential addition of hard spheres to a volume, *J. Chem. Phys.* **44**(10), 3888 (1966).
33. J. M. DeLaurentis and L. A. Romero, A Monte Carlo method for Poisson's equation, *J. Comput. Phys.* **90**, 123 (1990).